Electronic Supplementary Information

Hysteretic spin crossover in isomeric iron(II) complexes

Mark B. Bushuev,*[a,b] Viktor P. Krivopalov,[c] Elena B. Nikolaenkova,[c]
Katerina A. Vinogradova[a,b] and Yuri V. Gatilov[b,c]

[a] *Nikolaev Institute of Inorganic Chemistry, Siberian Branch of Russian Academy of Sciences, 3, Acad. Lavrentiev Ave., Novosibirsk, 630090, Russia, E-mail: bushuev@niic.nsc.ru, mark.bushuev@gmail.com; Fax: +7 383 330 94 89; Tel: +7 383 316 51 43.*

[b] *Novosibirsk State University, 2, Pirogova str., Novosibirsk, 630090, Russia.*

[c] *N. N. Vorozhtsov Novosibirsk Institute of Organic Chemistry, Siberian Branch of Russian Academy of Sciences, 9, Acad. Lavrentiev Ave., Novosibirsk, 630090, Russia.*

Table of contents

Chemistry

General

The synthesis of the complexes was carried out in deoxygenated EtOH under an inert atmosphere of argon using standard glovebox techniques. All reagents and solvents were commercially available and were used without additional purification. Elemental analysis (C, H, N) was performed with a EuroEA3000 analyzer using standard technique.

Synthesis of 2-(3,5-dimethyl-1*H*-pyrazol-1-yl)-4-methyl-6-(pyridin-2-yl)pyrimidine (*i*-L)

3,5-Dimethyl-1*H*-pyrazole-1-carboximidamide hydrochloride (1:1)[S1] and 1-(2-pyridinyl)-1,3-butanedione[S2] were synthesized by the published methods. (3,5-Dimethyl-1*H*-pyrazol-1-yl)formamidine hydrochloride (1.75 g, 10 mmol) was added to a solution of $NaOC_2H_5$ (10 mmol) in anhydrous ethanol (15 ml) and the mixture was stirred for 30 min. Then 1-(2-pyridinyl)-1,3-butanedione (1.63 g, 10 mmol) was added to the resulting suspension and the reaction mixture was refluxed with stirring for 20 h. The solvent was removed in vacuum and the crude product was purified by column chromatography on silica gel (eluent $CHCl_3$ – MeOH, 50 : 1). After column the semicrystal residue was treated with diethyl ether to give white crystalline product *i*-**L**. Yield: 0.38 g (14%), m.p. 162.5–164 °C. High-resolution mass spectrum, *m/z*: Calc. for $C_{15}H_{15}N_5$ 265.1322. Found 265.1321. ^1H NMR ($CDCl_3$, 400.13 MHz), δ (ppm): 8.70 (ddd, 1H, J = 4.8, 1.8, 0.8 Hz, 6-$H_{pyridine}$), 8.43 (dt, 1H, J = 7.8, 0.8 Hz, 3-$H_{pyridine}$), 8.08 (s, 1H, 5-$H_{pyrimidine}$), 7.85 (dt, 1H, J = 7.8, 1.8 Hz, 4-$H_{pyridine}$), 7.39 (ddd, 1H, J = 7.8, 4.8, 0.8 Hz, 5-$H_{pyridine}$), 6.05 (s, 1H, 4-$H_{pyrazole}$), 2.75 (d, 3H, J = 0.6 Hz, Me), 2.69 (s, 3H, Me), 2.34 (s, 3H, Me). ^{13}C NMR ($CDCl_3$, 125.75 MHz), δ (ppm): 170.90, 163.43, 157.16, 153.61, 151.06, 149.32 (CH), 142.43, 137.00 (CH), 125.34 (CH), 121.91 (CH), 113.34 (CH), 110.02 (CH), 24.60 (Me), 15.49 (Me), 13.84 (Me). IR spectrum ν_{max}/cm^{-1} (KBr pellet): 1597s, 1583vs, 1564s, 1543s, 1471s, 1450s, 1419vs, 1404s, 1376s, 1358s, 1313m, 1255m, 1230w, 1159w, 1117m, 1097w, 1043w, 1022w, 993m, 970m, 910w, 877w, 847w, 816m, 812m, 781m, 744m.

S1. G. G. Danagulyan and A. D. Mkrtchyan, *Haystani Kimiakan Handes,* 2005, **58**(1-2), 70–77.
S2. K. P. Strotmeyer, I. O. Frisky, R. Ott, H. Pritzkow and R. Kramer, *Supramolecular Chemistry*, 2003, **15**, 529–547.
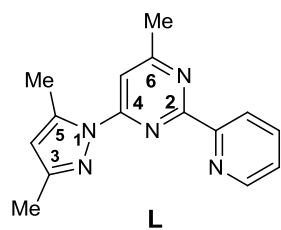
L

4-(3,5-dimethyl-1*H*-pyrazol-1-yl)-
6-methyl-2-(pyridin-2-yl)pyrimidine
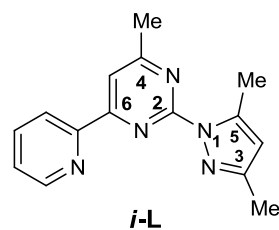
i-**L**

2-(3,5-dimethyl-1*H*-pyrazol-1-yl)-
4-methyl-6-(pyridin-2-yl)pyrimidine

Ligand L: ^{1}H NMR (CDCl$_3$, 400.13 MHz), δ (ppm): 8.84 (ddd, 1H, J = 4.8, 1.8, 0.8 Hz, 6-H$_{pyrydine}$), 8.39 (dt, 1H, J = 7.7, 0.8 Hz, 3-H$_{pyridine}$), 7.83 (dt, 1H, J = 7.7, 1.8 Hz, 4-H$_{pyridine}$), 7.77 (s, 1H, 5-H$_{pyrimidine}$), 7.38 (ddd, 1H, J = 7.7, 4.8, 1.0 Hz, 5-H$_{pyrydine}$), 6.04 (s, 1H, 4-H$_{pyrazole}$), 2.84 (s, 3H, Me), 2.69 (s, 3H, Me), 2.29 (s, 3H, Me).

Ligand *i*-L: ^{1}H NMR (CDCl3, 400.13 MHz), δ (ppm): 8.70 (ddd, 1H, J = 4.8, 1.8, 0.8 Hz, 6-H$_{pyrydine}$), 8.43 (dt, 1H, J = 7.8, 0.8 Hz, 3-H$_{pyridine}$), 7.85 (dt, 1H, J = 7.8, 1.8 Hz, 4-H$_{pyridine}$), 7.39 (s, 1H, 5-H$_{pyrimidine}$), 7.39 (ddd, 1H, J = 7.8, 4.8, 0.8 Hz, 5-H$_{pyrydine}$), 6.05 (s, 1H, 4-H$_{pyrazole}$), 2.75 (d, 3H, J = 0.6 Hz, Me), 2.69 (s, 3H, Me), 2.34 (s, 3H, Me).

Scheme S1. Structural formulae of L and *i*-L (with numbering scheme) and comparison of ^{1}H NMR data (CDCl$_3$, 400.13 MHz).

Synthesis of [Fe(*i*-L)$_2$](BF$_4$)$_2$ · EtOH (2^{LS} · EtOH)

A suspension of *i*-L (0.060 mmol, 15.9 mg) in EtOH (1 mL) was added to a solution of Fe(BF$_4$)$_2$·6H$_2$O (0.030 mmol, 10.2 mg) in EtOH (0.5 mL) in the presence of small amount of ascorbic acid. The solution turned dark violet. Dark violet prismatic crystals began to form immediately. In a day, the crystals were filtered off, washed with EtOH and dried in the ambient air. Yield: 18.2 mg (75 %). Elemental analysis for a freshly prepared sample (%), calcd for C$_{32}$H$_{36}$N$_{10}$B$_2$F$_8$FeO ([Fe(*i*-L)$_2$](BF$_4$)$_2$ · EtOH, 806.15): C 47.7, H 4.5, N 17.3; found C 47.6, H 4.3, N 17.4.

In the ambient air the crystals of **2^{LS} · EtOH** lose EtOH molecules (and probably sorbs H$_2$O molecules) transforming into **[Fe(*i*-L)$_2$](BF$_4$)$_2$ · yEtOH · zH$_2$O (2^{LS} · yEtOH · zH$_2$O**, y < 1, z > 0). At the same time the X-ray powder pattern of the product does not change significantly with respect to parent EtOH-containing phase. Elemental analysis for a sample after keeping at room temperature in the ambient air for a few months (%), calcd for C$_{32}$H$_{37}$N$_{10}$B$_2$F$_8$FeO ([Fe(*i*-L)$_2$](BF$_4$)$_2$ · H$_2$O, 778.11): C 46.3, H 4.1, N 18.0; found C 46.1, H 4.1, N 17.3; calcd for C$_{31}$H$_{35}$N$_{10}$B$_2$F$_8$FeO$_{1.5}$ ([Fe(*i*-L)$_2$](BF$_4$)$_2$ · H$_2$O · 0.5EtOH, 801.13): C 46.5, H 4.5, N 17.5; found C 46.1, H 4.1, N 17.3. This tendency shows that EtOH molecules easily evaporate even at room temperature.

Synthesis of [FeL$_2$](BF$_4$)$_2$ · yEtOH · zH$_2$O (1$^{E/LS}$ · yEtOH · zH$_2$O)

A solution of L (0.060 mmol, 15.9 mg) in EtOH (0.5 mL) in the presence of Triton (20 μL) was added to a solution of Fe(BF$_4$)$_2$·6H$_2$O (0.030 mmol, 10.2 mg) in EtOH (0.5 mL) in the presence of Triton-100 (20 μL) and small amount of ascorbic acid. The solution turned dark red and immediately treated by ultrasound for 10 min. This procedure resulted in the formation of dark red powder. The powder was filtered off, washed with EtOH and dried in the ambient air. Yield: 14.3 mg. Elemental analysis for a freshly prepared sample (%), calcd for C$_{30.8}$H$_{33.2}$N$_{10}$B$_2$F$_8$FeO$_{0.8}$ ([FeL$_2$](BF$_4$)$_2$ · 0.4EtOH · 0.4H$_2$O, 785.75): C 47.1, H 4.3, N 17.8; found C 47.2, H 3.9, N 17.8.

Crystallography

Crystallographic data for 2^LS·EtOH

Formula $C_{32}H_{36}B_2F_8FeN_{10}O$, M = 806.18, monoclinic, space group $P2_1/c$, a = 8.8221(5), b = 14.8811(7), c = 27.4419(15) Å, β = 93.482(2)°, V = 3596.0(3) Å^3, Z = 4, D_{calc} = 1.489 g·cm^{-3}, μ = 0.504 mm^{-1}, min/max transmission = 0.786/0.862, θ_{max} = 27.5°, measured 53148, unique 8152 (R_{int} = 0.0260), observed [$I_o > 2\sigma(I)$] 6565 reflections, R_1 = 0.0685 (I_o), wR_2 = 0.1941 (all), Gof = 0.949, $\Delta\rho_{max}$ = 1.47, $\Delta\rho_{min}$ = -0.90 e·Å^{-3}, CCDC 1845013. One tetrafluoroborate ion is disordered over three positions with occupancies 0.337(10): 0.310(7): 0.353(11). The ethanol molecule is also disordered over two positions with occupancies 0.720(7):0.280(7). Disordered molecules were refined in isotropic model with geometrical restraints. Removing anions and EtOH molecules using the SQUEEZE procedure in the PLATON program[S3] leads to a reduction in the R factor to R = 0.0438 (I_o).

S3   A. L. Spek, *Acta Cryst.*, 2015, **C71**, 9-18.

Table S1. Comparison of selected bond lengths (Å) and angles (°) in the crystal structures of [Fe(*i*-L)$_2$](BF$_4$)$_2$·EtOH (**2^LS · EtOH**) and [FeL$_2$](BF$_4$)$_2$·0.41EtOH·0.4H$_2$O (**1^E/LS · 0.41EtOH · 0.4H$_2$O**).

Bond length	2^LS · EtOH	1^E/LS · 0.41EtOH · 0.4H$_2$O
Fe(1)–N(2)	1.884(3)	1.889(3)
Fe(1)–N(3)	1.986(3)	1.983(4)
Fe(1)–N(5)	2.008(3)	2.005(4)
Fe(1)–N(7)	1.880(3)	1.888(3)
Fe(1)–N(8)	1.982(3)	1.982(4)
Fe(1)–N(10)	2.001(3)	1.998(4)
Angle		
N(2)–Fe(1)–N(3)	80.22(12)	80.68(15)
N(2)–Fe(1)–N(5)	79.45(12)	79.06(14)
N(2)–Fe(1)–N(7)	179.36(11)	179.21(15)
N(2)–Fe(1)–N(8)	99.25(11)	99.47(15)
N(2)–Fe(1)–N(10)	100.76(11)	100.51(15)
N(3)–Fe(1)–N(5)	159.67(12)	159.64(14)
N(3)–Fe(1)–N(7)	99.93(12)	98.63(15)
N(3)–Fe(1)–N(8)	93.24(11)	93.29(15)
N(3)–Fe(1)–N(10)	90.31(11)	89.38(15)
N(5)–Fe(1)–N(7)	100.40(11)	101.65(15)
N(5)–Fe(1)–N(8)	90.17(11)	88.20(15)
N(5)–Fe(1)–N(10)	93.31(11)	96.13(15)
N(7)–Fe(1)–N(8)	80.12(11)	80.91(15)
N(7)–Fe(1)–N(10)	79.87(11)	79.10(15)
N(8)–Fe(1)–N(10)	159.99(11)	160.01(15)
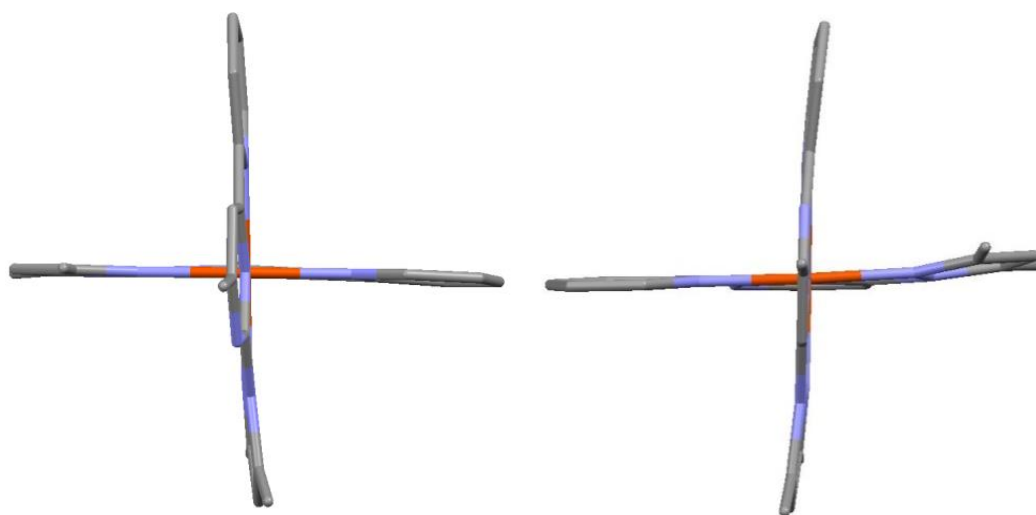
Figure S1. Structural distortions exhibited by the cations in the structures of **2$^{\text{LS}}$·EtOH** (left, φ = 179.4°, θ = 85.9°) and **1$^{\text{E/LS}}$·yEtOH·zH$_2$O** (right, φ = 179.2°, θ = 83.3°). Hydrogen atoms are omitted for clarity.

Packing of $1^{E/LS} \cdot yEtOH \cdot zH_2O$
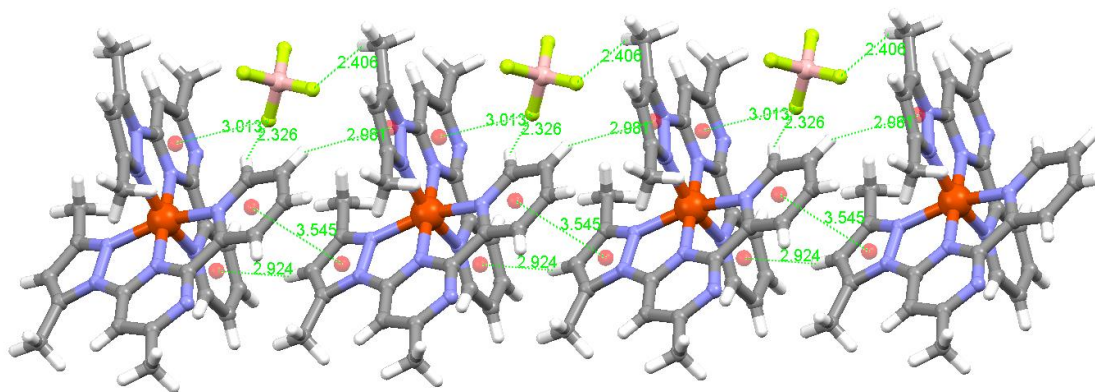
Figure S2. 1D chain in the structure of $1^{E/LS} \cdot yEtOH \cdot zH_2O$.
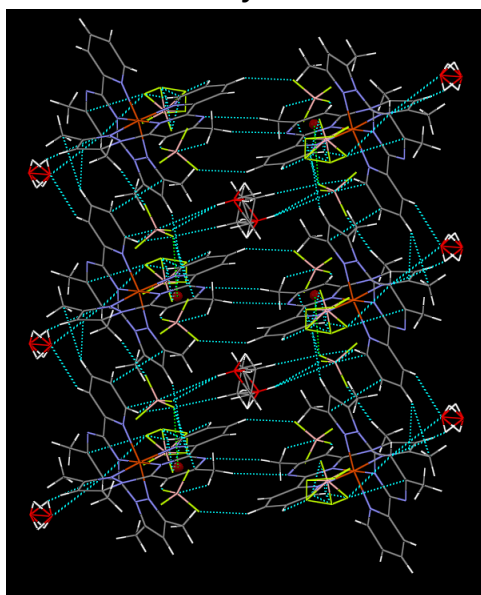
Figure S3. Short contacts linking two 1D chains into a ribbon in the structure of $1^{E/LS} \cdot yEtOH \cdot zH_2O$.
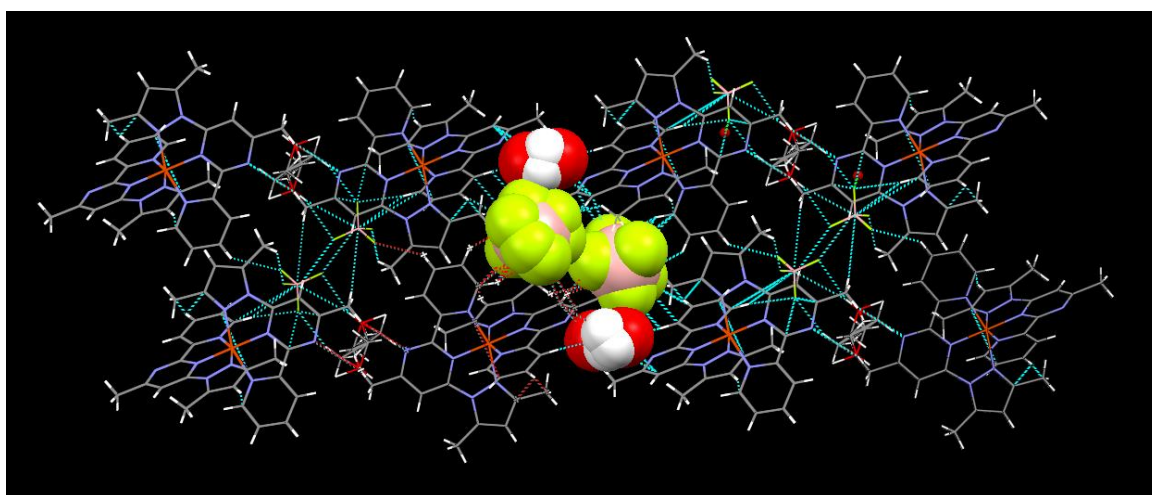
Figure S4. Disordered BF_4^- ions and H_2O molecules in the space-filling model between the ribbons (view along the ribbons, four ribbons are shown) in the structure of $1^{E/LS} \cdot yEtOH \cdot zH_2O$.

Packing of 2^{LS}·EtOH
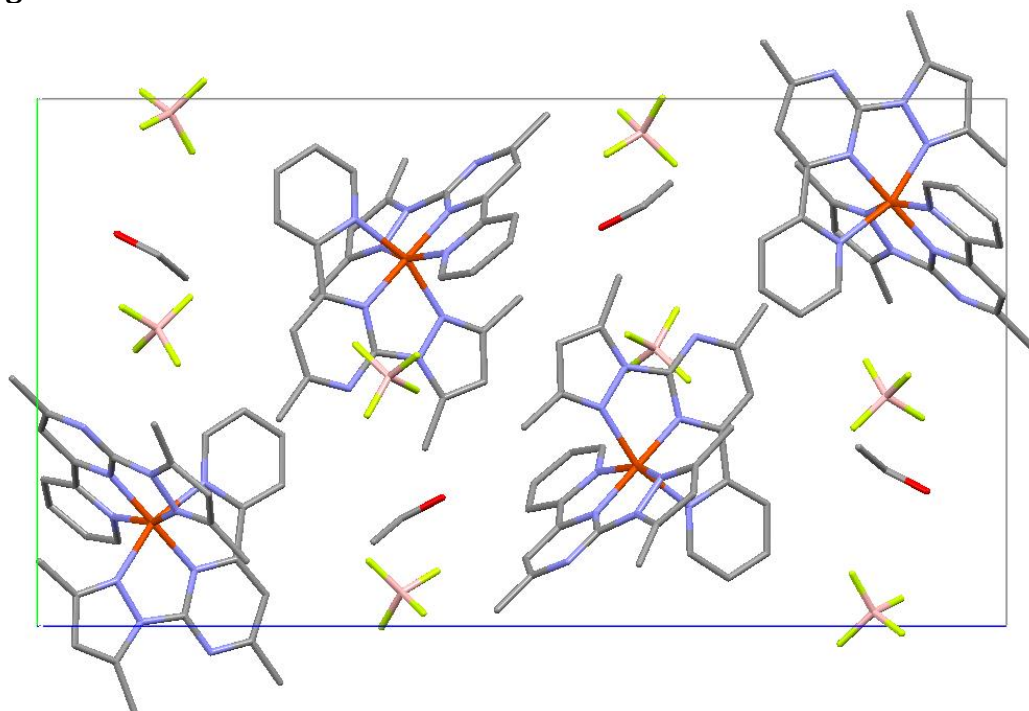
Figure S5. Packing diagram of **2^{LS}·EtOH**, view along the *a*-axis.
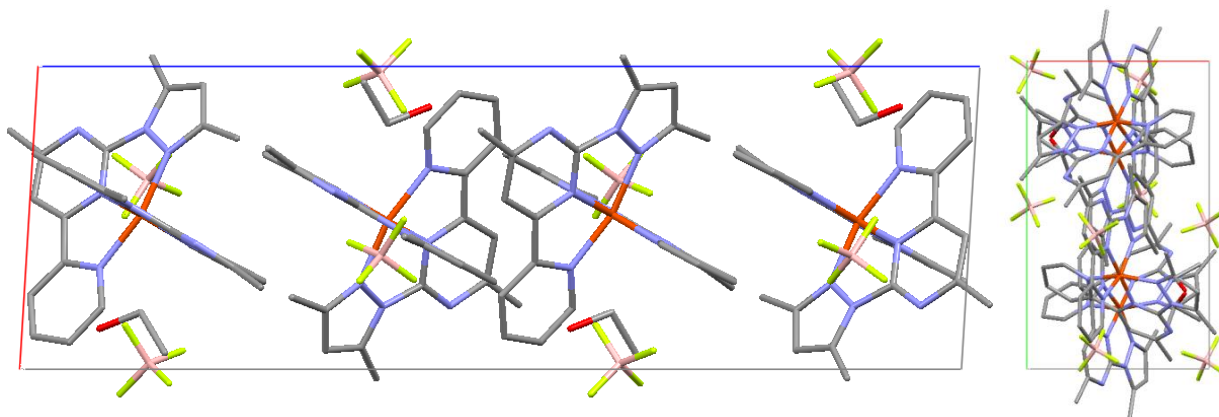
Figure S6. Packing diagram of **2^{LS}·EtOH**, view along the *b*-axis (left) and *c*-axis (right).
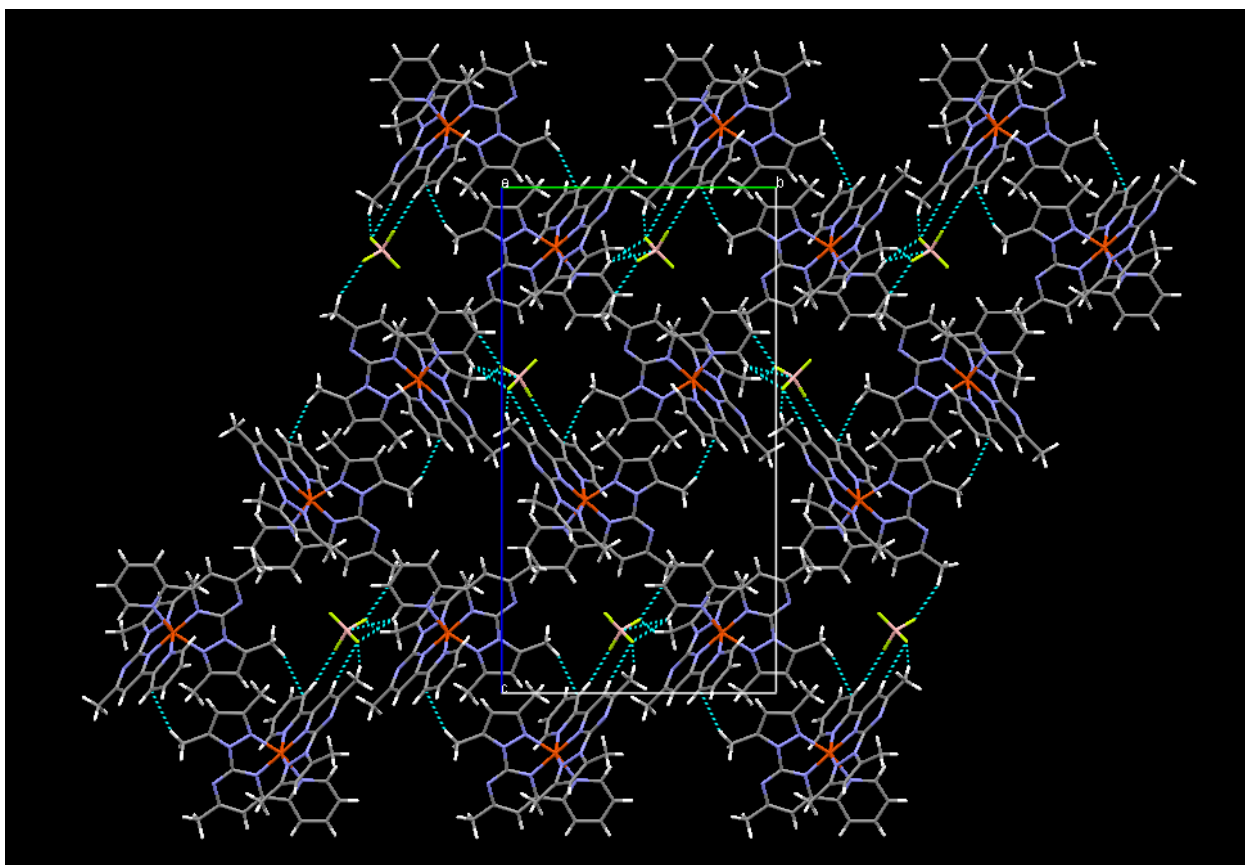
Figure S7. A 2D-layer in the structure of **2^{LS} · EtOH**. View along the *a*-axis.
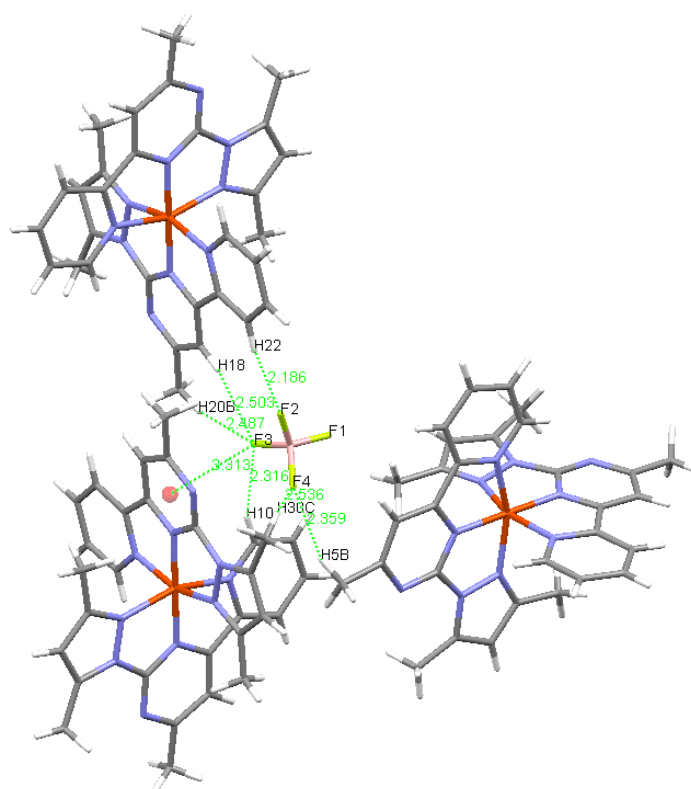
Figure S8. Non-disordered anion BF_4^- in the structure of **2^{LS} · EtOH** (C–H…F contacts and lone-pair…π interactions are shown).
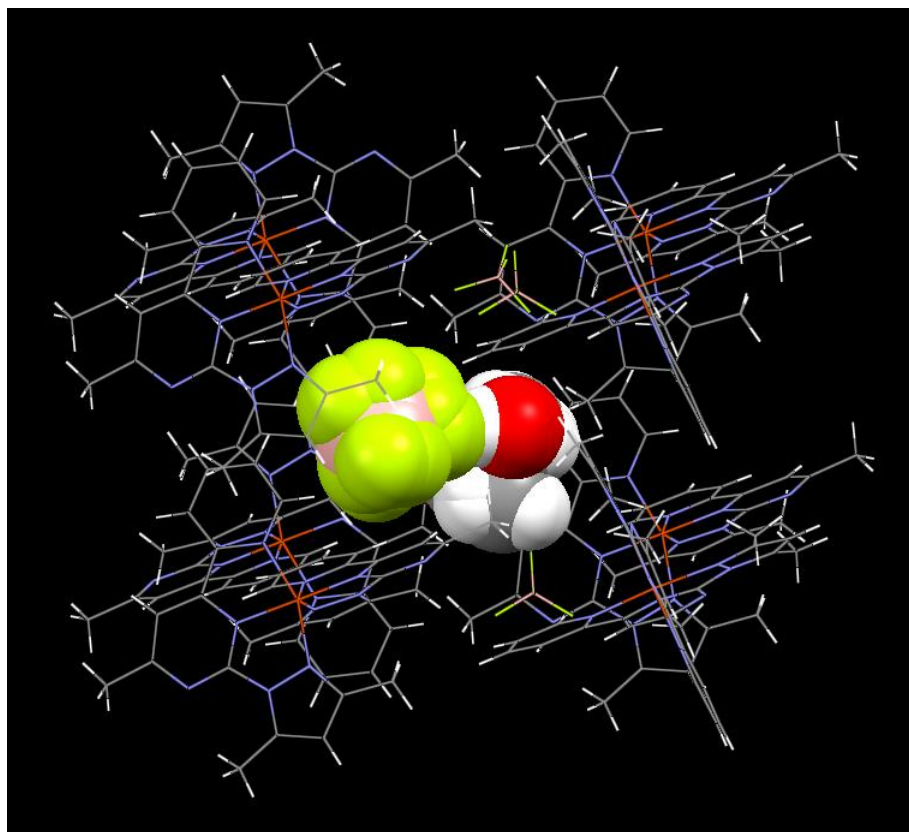
Figure S9. Disordered BF_4^- and EtOH (shown in the space-filling model) and neighbouring $[Fe(i\text{-}L)]^{2+}$ dications in the structure of **2^{LS} · EtOH**.
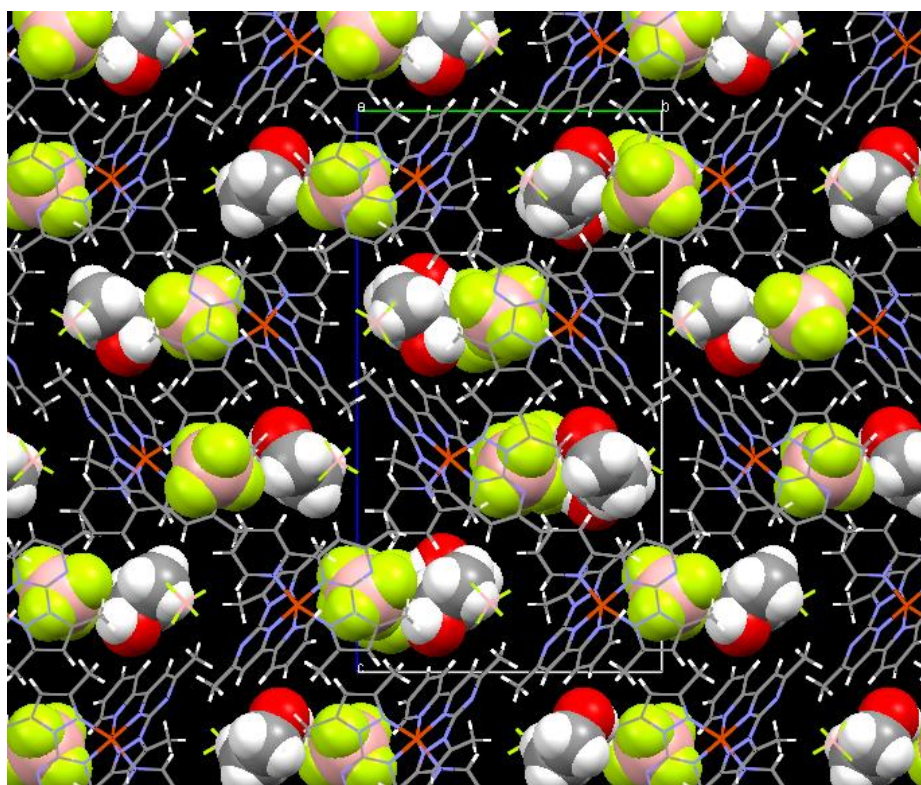
Figure S10. Crystal packing of **2^{LS} · EtOH** showing relative arrangement of disordered ethanol molecules and BF_4^- ions in the space-filling model. View along the *a*-axis.
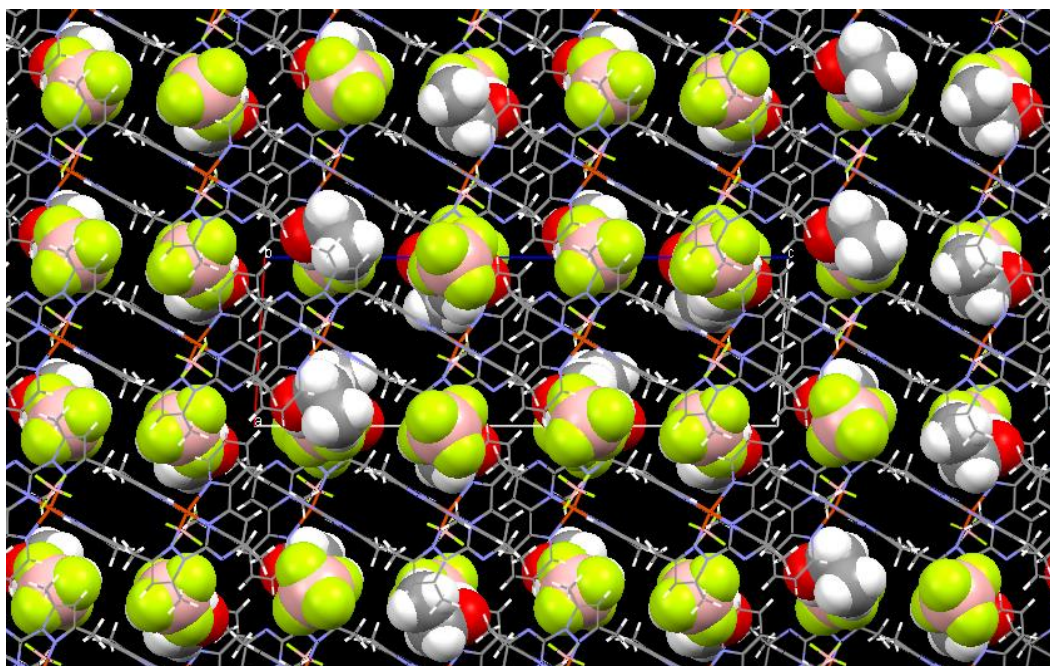
Figure S11. Crystal packing of **2LS · EtOH** showing relative arrangement of disordered ethanol molecules and BF_4^- ions in the space-filling model. View along the *b*-axis.
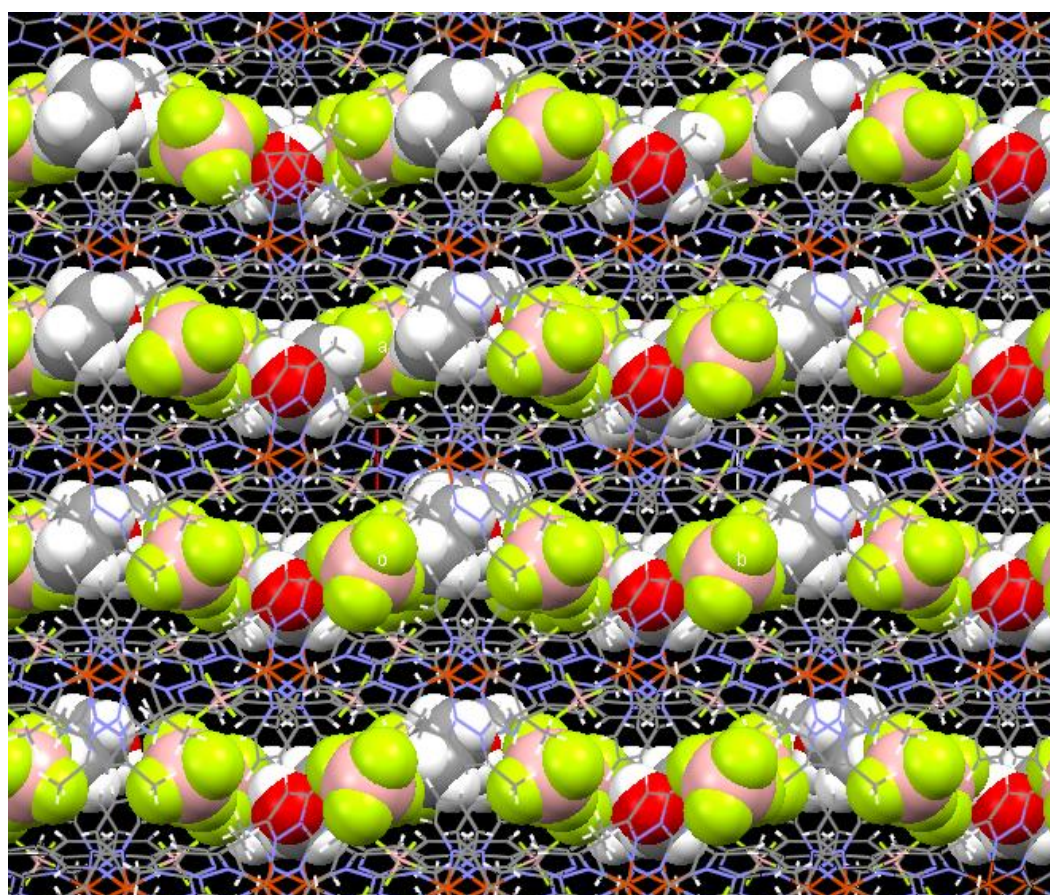
Figure S12. Crystal packing of **2LS · EtOH** showing relative arrangement of disordered ethanol molecules and BF_4^- ions in the space-filling model. View along the *c*-axis.

X-ray powder diffraction

XPRD analysis of polycrystals was performed on Shimadzu XRD-7000 diffractometer (Cu-K_α radiation, Ni – filter, 0.03° 2θ step, 5s per point). The samples were slightly ground with hexane in an agate mortar and the resulting suspension was deposited on the polished side of a standard quartz sample holder. Smooth thin layers were formed after drying.
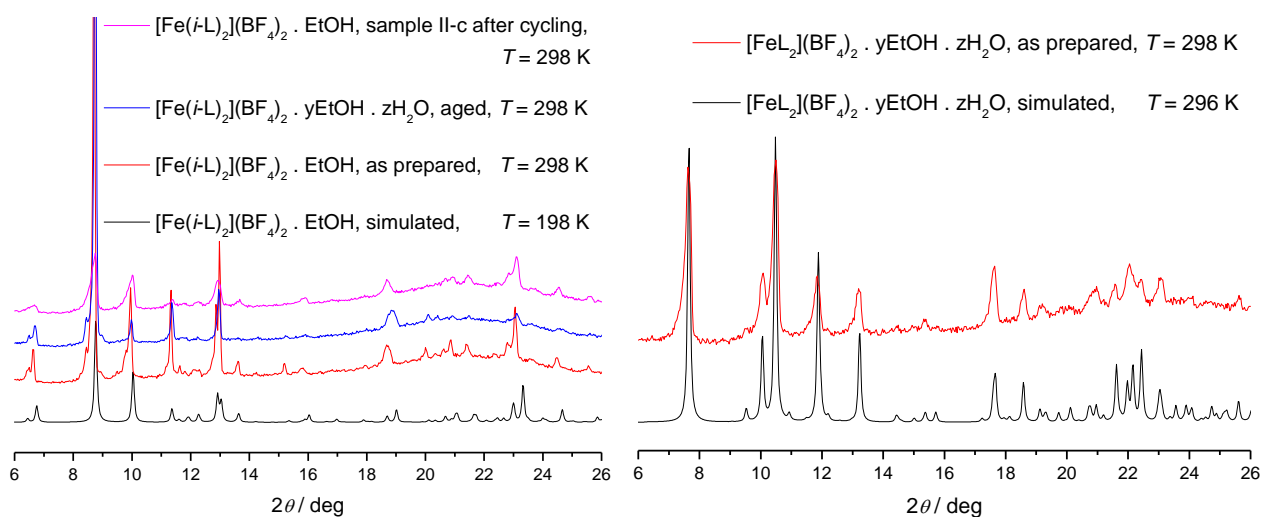
Figure S13. XRPD patterns of [Fe(i-L)₂](BF₄)₂ · EtOH, [Fe(i-L)₂](BF₄)₂ · yEtOH · zH₂O and [Fe(L)₂](BF₄)₂ · yEtOH · zH₂O.

IR-spectroscopy

IR absorption spectra were recorded on a Scimitar FTS 2000 spectrometer.
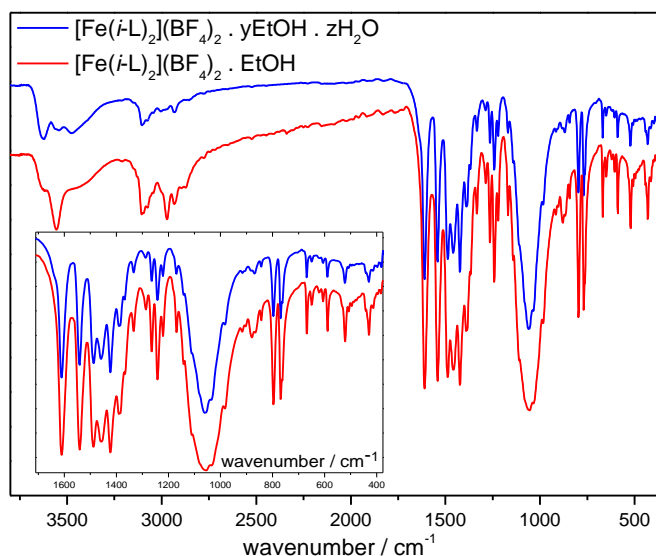
Figure S14. IR spectra of $[Fe(i\text{-}L)_2](BF_4)_2 \cdot EtOH$ and $[Fe(i\text{-}L)_2](BF_4)_2 \cdot yEtOH \cdot zH_2O$ in KBr.

Thermal analysis

Thermal analysis of $[Fe(i\text{-}L)_2](BF_4)_2 \cdot EtOH$ (**$2^{LS} \cdot EtOH$**), $[Fe(i\text{-}L)_2](BF_4)_2 \cdot yEtOH \cdot zH_2O$ (**$2^{LS} \cdot yEtOH \cdot zH_2O$**) and $[FeL_2](BF_4)_2 \cdot yEtOH \cdot zH_2O$ (**$1^{E/LS} \cdot yEtOH \cdot zH_2O$**) was performed on NETZSCH TG 209 F1 instrument (Al_2O_3 crucible, He flow, heating rate 10 K min^{-1}).
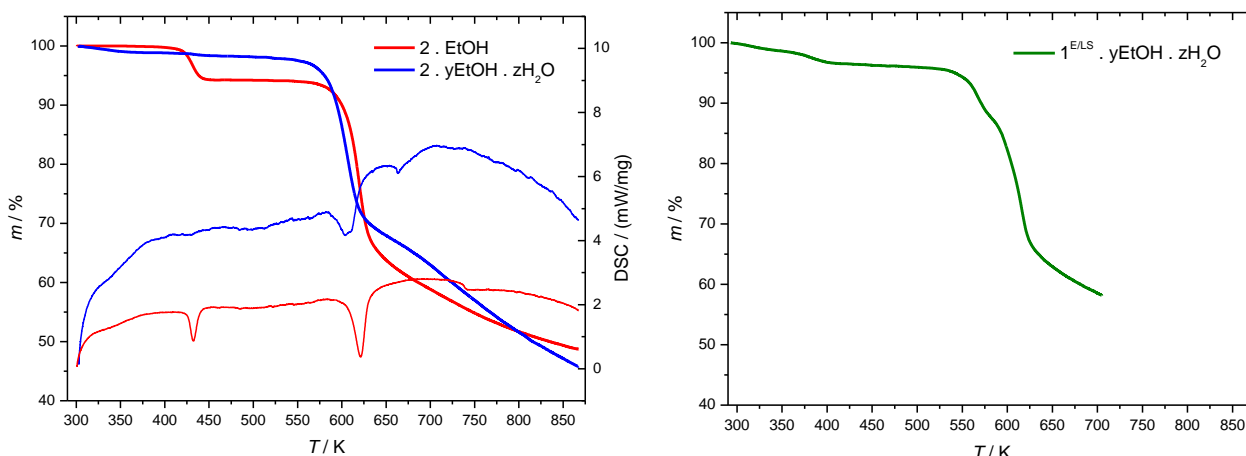
Figure S15. TG curves for the complexes $[Fe(i\text{-}L)_2](BF_4)_2 \cdot EtOH$ (**$2^{LS} \cdot EtOH$**) and $[Fe(i\text{-}L)_2](BF_4)_2 \cdot yEtOH \cdot zH_2O$ (**$2^{LS} \cdot yEtOH \cdot zH_2O$**) (left) and $[FeL_2](BF_4)_2 \cdot yEtOH \cdot zH_2O$ (**$1^{E/LS} \cdot yEtOH \cdot zH_2O$**) (right).

Exact amount of outerspheric solvent molecules is difficult to determine by TGA because these molecules (especially EtOH) evaporate from the samples even at room temperature.

Scanning electron microscopy
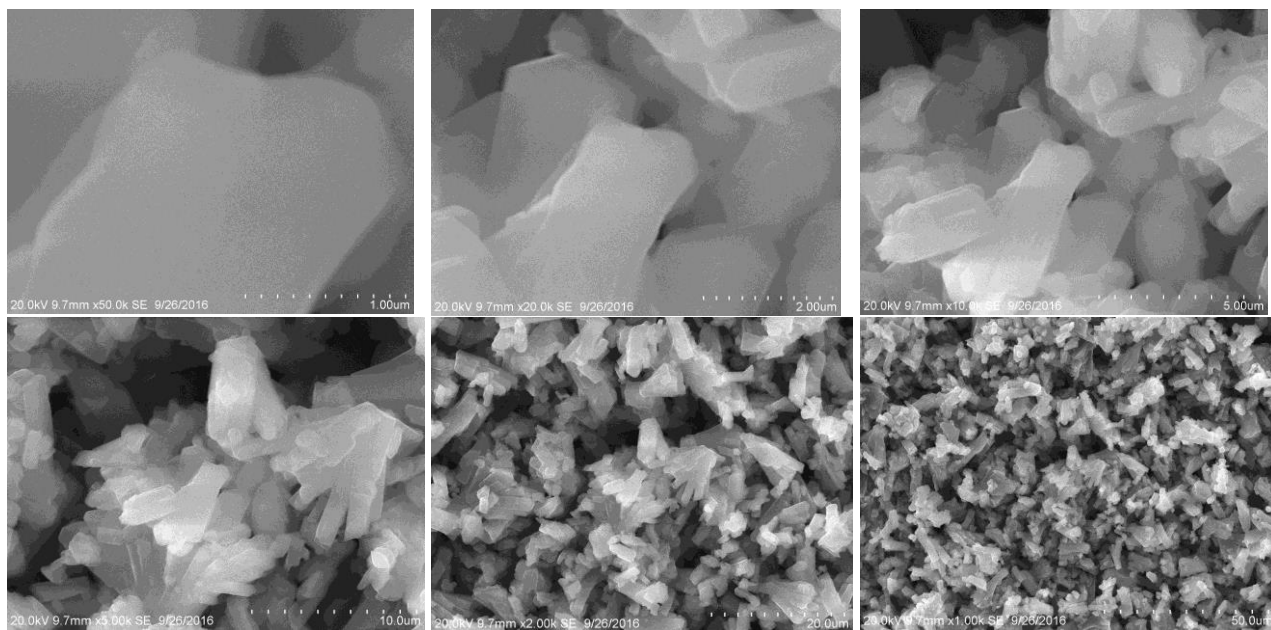
Figure S16. SEM images of $\mathbf{1^{E/LS} \cdot y EtOH \cdot z H_2 O}$.

Magnetochemistry

Measurements of the magnetic susceptibilities of the complexes were performed in the field of 9.09 kOe. Small quartz ampoules were used for the measurements. Samples I, II-b and II-c were sealed in the ampoules immediately after the synthesis. The sample II-d was sealed on 53rd day after the synthesis. The molar magnetic susceptibilities of the complexes (χ_M) were corrected for the diamagnetic contributions of the atoms using the Pascal additive scheme and for the diamagnetism of the ampoules. The heating/cooling rate was 0.5 – 4 K min^{-1}. The spin transition temperatures $T_c\uparrow$ and $T_c\downarrow$ were determined in by the maximum value of d($\chi_M T$)/dT.

Table S2. Magnetochemical data.

Sample	Conditions / formula / m/V	Cycle	Day of cycling	Rate, K/min	$T_c\uparrow$, K	$T_c\downarrow$, K	ΔT, K
II-a	Vacuum, **2 · EtOH**	1	1st	4	≈415	≈325	
II-b	Sealed ampoule, **2 · EtOH** 0.0463 mg/μL	1	1st	4	≈405	≈325	≈80
		2	21st	2	374	355	19
		3	35th	1	368	356	12
		4	84th	1.5	373	357	16
		5	113rd	2	374	356	18
II-c	Sealed ampoule, **2 · EtOH** 0.0304 mg/μL	1	1st	4	≈405	≈325	≈80
		2	22nd	1	374	330	44
		3	23rd	1	374	330	44
II-d	Sealed ampoule, **2 · yEtOH · zH₂O** (sealed on the 53rd day after the synthesis) 0.0349 mg/μL	1	1st	4	≈400	≈320	80
		2	35th	2	374	330	44
		3	42nd	2	368	335	33
		4	56th	1	362	338	24
		5	105th	1.5	368	338	30
I	Sealed ampoule, **1 · yEtOH · zH₂O** 0.0435 mg/μL	1	1st	4	≈395	340 (kin.)	
		2	31st	2	389	352	37
		3	38th	1	381	357	24
		4	45th	0.5	377	356	21
		5	52nd	0.5	376	357	19
		6	66th	2	386	354	32
		7	71st	2	384	354	30
		8	77th	1	381	356	25
		9	78th		380 (kin.)	354 (kin.)	
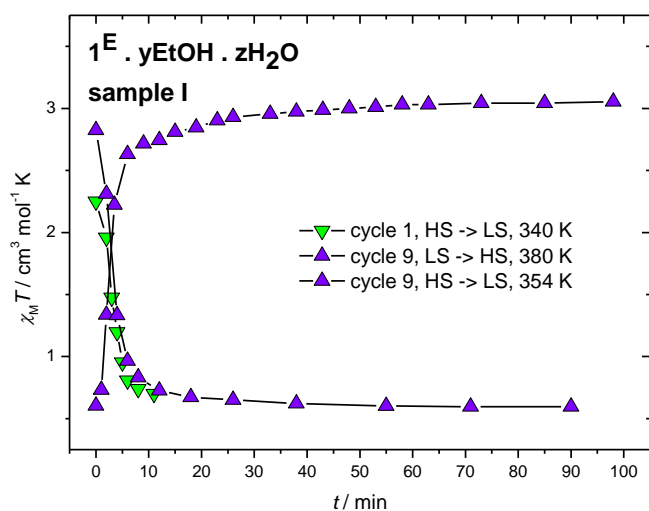
Figure S17. Isothermal kinetic curves for $1^E \cdot yEtOH \cdot zH_2O$.

Reaction models

Table S3. List of reaction models.

model	$f(\alpha)$
F1	$(1 - \alpha)$
F2	$(1 - \alpha)^2$
F3	$(1 - \alpha)^3$
Fn	$(1 - \alpha)^n$
R2	$2(1 - \alpha)^{1/2}$
R3	$3(1 - \alpha)^{2/3}$
D1	$1/(2\alpha)$
D2	$-[1/\ln(1 - \alpha)]$
D3	$[3(1 - \alpha)^{2/3}]/[2(1 - (1 - \alpha)^{1/3})]$
D4	$3/[2((1 - \alpha)^{-1/3} - 1)]$
B1	$\alpha(1 - \alpha)$
Bna	$\alpha^a(1 - \alpha)^n$
C1B	$(1 - \alpha)(1 + K_{cat}\alpha)$
CnB	$(1 - \alpha)^n(1 + K_{cat}\alpha)$
A2	$2(1 - \alpha)[-\ln(1 - \alpha)]^{1/2}$
A3	$3(1 - \alpha)[-\ln(1 - \alpha)]^{2/3}$
A4	$4(1 - \alpha)[-\ln(1 - \alpha)]^{3/4}$
An	$n(1 - \alpha)[-\ln(1 - \alpha)]^{(n - 1)/n}$

The function $f(\alpha)$ describes the dependence of the rate of a topochemical reaction on the extent of conversion, α.